



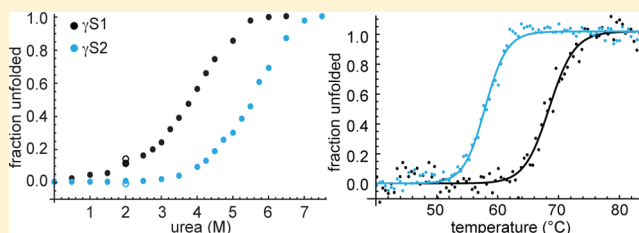
# $\gamma$ S-Crystallin Proteins from the Antarctic Nototheniid Toothfish: A Model System for Investigating Differential Resistance to Chemical and Thermal Denaturation

Carolyn N. Kingsley,<sup>†</sup> Jan C. Bierma,<sup>‡</sup> Vyvy Pham,<sup>†</sup> and Rachel W. Martin<sup>\*,†,‡</sup>

<sup>†</sup>Department of Chemistry, University of California—Irvine, 1102 Natural Sciences 2, Irvine, California, 92697-2025, United States

<sup>‡</sup>Department of Molecular Biology and Biochemistry, University of California—Irvine, 3205 McGaugh Hall, Irvine, California 92697, United States

**ABSTRACT:** The  $\gamma$ S1- and  $\gamma$ S2-crystallins, structural eye lens proteins from the Antarctic toothfish (*Dissostichus mawsoni*), are homologues of the human lens protein  $\gamma$ S-crystallin. Although  $\gamma$ S1 has the higher thermal stability of the two, it is more susceptible to chemical denaturation by urea. The lower thermodynamic stability of both toothfish crystallins relative to human  $\gamma$ S-crystallin is consistent with the current picture of how proteins from organisms endemic to perennially cold environments have achieved low-temperature functionality via greater structural flexibility. In some respects, the sequences of  $\gamma$ S1- and  $\gamma$ S2-crystallin are typical of psychrophilic proteins; however, their amino acid compositions also reflect their selection for a high refractive index increment. Like their counterparts in the human lens and those of mesophilic fish, both toothfish crystallins are relatively enriched in aromatic residues and methionine and exiguous in aliphatic residues. The sometimes contradictory requirements of selection for cold tolerance and high refractive index make the toothfish crystallins an excellent model system for further investigation of the biophysical properties of structural proteins.



## INTRODUCTION

Proteins require optimized stability and flexibility to perform their biological roles, including interacting with binding partners, responding to their environment and resisting aggregation. Protein function depends on both structure and dynamics; making the folded state of a protein more stable by rigidifying it does not necessarily lead to enhanced functionality.<sup>1</sup> Comparisons among homologous proteins from thermophilic, mesophilic, and psychrophilic organisms have often shown that these proteins are comparably flexible when each is considered at its physiologically relevant temperature, even though in thermodynamic terms adaptation to higher temperature often correlates with higher stability.<sup>2</sup> The crystallins, the structural proteins of the eye lens, are unusually stable and thus present an attractive model system for studying questions of protein stability. These proteins create the high refractive index necessary for this specialized tissue to focus light on the retina; the concentration and distribution of the different crystallins determine the refractive index gradient of the lens. Unlike in land animals, where the air–water interface at the cornea provides a significant amount of focusing power, in aquatic organisms the crystallins alone produce the refractive capability of the eye. Fish lenses are therefore more spherically shaped than those of land animals and have both increased protein concentrations and greater protein refractivity in comparison to their terrestrial counterparts.<sup>3</sup> While the crystallin concentrations in mammalian lenses can reach up

to 450 mg·mL<sup>-1</sup>, lenses belonging to aquatic organisms reach up to 1000 mg·mL<sup>-1</sup>.<sup>4,5</sup>

In vertebrates there are two common types of lens proteins: the  $\beta\gamma$ -crystallins, which are primarily structural, and the  $\alpha$ -crystallins, which have an additional function of binding damaged structural proteins and preventing aggregation.<sup>6</sup> These two protein families have different evolutionary histories and distinct structures.<sup>7</sup> The  $\alpha$ -crystallins are believed to have resulted from the gene duplication of an ancestral  $\alpha$ -crystallin domain; these proteins are closely related to each other and to other chaperone proteins.<sup>8,9</sup> The structural crystallins, including the taxon-specific crystallins found in many organisms, and the  $\beta\gamma$ -crystallins that are the focus of this study have been recruited from diverse abundant, soluble proteins via gene sharing or duplication often followed by selection for increased refractivity of the protein itself.<sup>10–12</sup> The  $\beta\gamma$ -crystallin superfamily, which is characterized by two double Greek key domains, is thought to be derived from a calcium-binding motif that existed before the evolution of eye lenses,<sup>13</sup> as evidenced by similarity to calcium-binding proteins in sequences from archaea,<sup>14</sup> slime mold,<sup>15</sup> and urochordate.<sup>16</sup> The urochordate (*Ciona intestinalis*) protein in particular is highly similar to the vertebrate members of the family, but with two notably different features: it has only one domain rather than two, and

**Received:** September 10, 2014

**Revised:** November 4, 2014

**Published:** November 5, 2014

it contains two calcium binding sites. Despite this common evolutionary history, functional mammalian lens proteins lack calcium-binding activity.<sup>17</sup> A study of the structure and dynamics of zebrafish (*Danio rerio*)  $\gamma$ M7-crystallin by solution-state NMR has revealed a potentially general unfolding pathway for all  $\beta\gamma$ -crystallin domains.<sup>18</sup> Although this protein has the same overall fold as the mammalian  $\beta\gamma$ -crystallins, there are significant primary sequence differences, including enhanced methionine content as well as the absence of some of the tryptophan residues that are strongly conserved in mammals. In teleost fishes, the  $\gamma$ M-crystallins are the most common structural proteins in the lens, while  $\beta$ -crystallins are more common in humans.<sup>19</sup> Although  $\gamma$ S-crystallins are a relatively minor subclass in both cases, they were chosen as the focus of this study because their amino acid sequences are strongly conserved among all vertebrates and because of their ability to resist cold cataract.<sup>20</sup>

Crystallins, particularly in fish lenses, are enriched in highly polarizable amino acids and exiguous in aliphatic amino acids as a result of their selection for high refractive index.<sup>21</sup> This selective pressure can potentially work against the selective pressure for cold tolerance, which favors a relatively high proportion of hydrophobic residues on the surface. In comparisons of crystallin proteins from different environments, two notions of protein stability are relevant.<sup>22</sup> The thermodynamic stability,  $\Delta G^\circ$  of unfolding, is the difference in Gibbs free energy between the folded and unfolded states, measured by reversible denaturation of the protein.<sup>23</sup> The unfolding temperature  $T_m$  is measured by (usually irreversible) direct thermal denaturation.<sup>24</sup> Although they are not directly comparable, the thermal and chemical stabilities of similar proteins are often positively correlated; in a series of homologs or variants, it is common for the ordering of thermal and chemical denaturation resistance to follow the same ordinal ranking. In the case of the eye lens crystallins from the Antarctic toothfish (*Dissostichus mawsoni*), comparing the thermal and chemical stabilities of two closely related proteins can potentially provide insight into the different sequence characteristics related to their two major functions: cold tolerance and high refractive index.

The Antarctic toothfish lives in the cold waters of the Southern Ocean, where temperatures can be as cold as  $-2^\circ\text{C}$ . This large fish has a relatively long lifespan ( $\sim 50$  years). Its lens proteins are therefore resistant to both age-related loss of solubility and the formation of cold cataract.<sup>25</sup> *D. mawsoni* has two  $\gamma$ S-crystallin paralogs,  $\gamma$ S1- and  $\gamma$ S2-crystallin (abbreviated T $\gamma$ S1 and T $\gamma$ S2 throughout), with a sequence identity of 60%. Protein turnover is very low in the eye lens, requiring the crystallins to maintain their stability and solubility over the whole lifespan of the organism. In mesophilic organisms, high stability corresponds to a high thermal denaturation temperature and high  $\Delta G^\circ$  of unfolding. Quantitative thermodynamic studies of cold-adapted proteins so far have generally found decreased thermodynamic stability.<sup>26–29</sup> In general, psychrophilic proteins are characterized by decreased core hydrophobicity, exiguous isoleucine content, increased surface hydrophobicity, fewer total charged residues, increased surface charge, a lower arginine/lysine ratio, weaker interdomain and intersubunit interactions, decreased secondary structure content, more and longer loops, more glycine residues, fewer and weaker metal-binding sites, fewer disulfide bonds, fewer electrostatic interactions, and increased conformational entropy of the unfolded state.<sup>30</sup> Some of these adaptations conflict with

the primary optical function of the  $\gamma$ -crystallins, for which highly polarizable amino acids are selected. Quantitatively, this is described by the refractive index increment  $dn/dc$ , the change in refractive index with concentration. Although this can be empirically determined, for proteins it is often assumed to be described by a simple additive model in which only the amino acid content is important for determining  $dn/dc$  for the entire protein molecule.<sup>11</sup>

Here we compare the thermal and chemical stabilities of *D. mawsoni*  $\gamma$ S1- and  $\gamma$ S2-crystallins in light of these competing functions. Although these proteins have comparable values for  $\Delta G^\circ$  of unfolding, surprisingly, T $\gamma$ S1 is more susceptible to thermal denaturation while T $\gamma$ S2 is more readily unfolded with urea. For related proteins, these quantities are typically positively correlated with each other and with overall thermodynamic stability. The differential resistance to thermal and chemical unfolding in this system underscores the different mechanisms of unfolding involved and the intramolecular interactions involved in resistance to them.

## ■ EXPERIMENTAL METHODS

### Gene Construction, Expression, and Purification.

Plasmids containing the cDNA sequences of the human  $\gamma$ S-crystallin (h $\gamma$ S) and *D. mawsoni*  $\gamma$ S1 (GenBank, DQ143971.1) and  $\gamma$ S2 (GenBank, DQ143972.1) genes<sup>31</sup> were purchased from Blue Heron Biotech, LLC. (Bothell, WA). Each gene was flanked by regions containing restriction sites for NcoI and XhoI, an N-terminal 6 $\times$  His tag, and a TEV cleavage sequence (ENLFGQ) with the N-terminal methionine of h $\gamma$ S, T $\gamma$ S1, and T $\gamma$ S2 replaced by the final glycine in the cleavage sequence. The biophysical experiments described below were performed without removing the N-terminal 6 $\times$  His tag. The toothfish crystallin genes were amplified using oligonucleotide primers purchased from Sigma-Aldrich (St. Louis, MO), and the resulting gene products were individually cloned into pET28a-(+) vectors (Novagen, Darmstadt, Germany). h $\gamma$ S, T $\gamma$ S1, and T $\gamma$ S2 were overexpressed in Rosetta (DE3) *Escherichia coli* using standard IPTG-induced overexpression protocols at  $25^\circ\text{C}$  in standard Luria broth (LB). Cells were allowed to grow for 16–24 h after induction. The cells were lysed by sonication, and cell debris was removed by centrifugation. His-TEV-h $\gamma$ S, His-TEV-T $\gamma$ S1, and His-TEV-T $\gamma$ S2 were purified on a Ni-NTA column (Applied Biosystems, Foster City, CA). The pure protein was collected from the column elution fraction and then dialyzed extensively against 10 mM phosphate buffer, pH 6.9, for all experiments.

**Circular Dichroism.** Purified T $\gamma$ S1 and T $\gamma$ S2 were diluted to  $0.125\text{ mg}\cdot\text{mL}^{-1}$  with 10 mM phosphate buffer at pH 6.9 for the collection of full circular dichroism (CD) spectra and to  $0.25\text{ mg}\cdot\text{mL}^{-1}$  with 10 mM phosphate buffer at pH 6.9, 150 mM NaCl, and 1 mM DTT for unfolding experiments. Measurements were taken on a J-810 spectropolarimeter (JASCO, Easton, MD) equipped with a thermal controller. For unfolding measurements, the samples were heated at a rate of  $2^\circ\text{C}\cdot\text{min}^{-1}$ . For thermal denaturation curves, the CD at 218 nm was monitored and the curves were fit to a two-state equilibrium unfolding model to determine the thermal denaturation temperature ( $T_m$ ).

**Fluorescence Spectroscopy.** UV fluorescence measurements were made on T $\gamma$ S1 and T $\gamma$ S2 at a concentration of  $0.075\text{ mg}\cdot\text{mL}^{-1}$  in 10 mM phosphate buffer, pH 6.9. Samples for chemical unfolding curves were prepared with increasing concentrations of 10 M urea (Fisher Scientific, Waltham, MA).

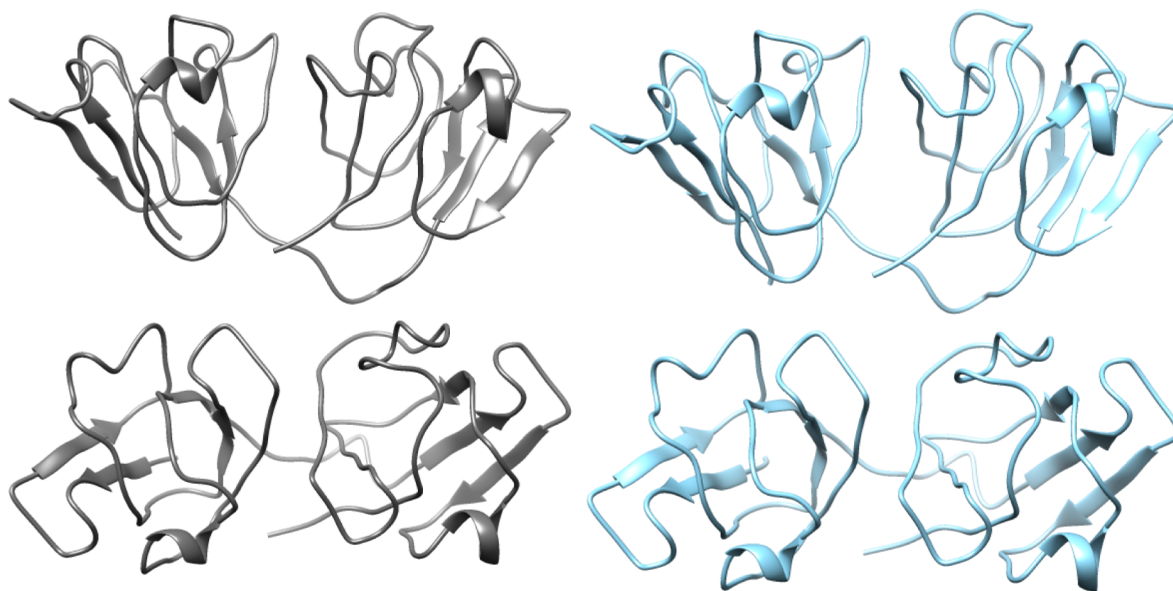


**Figure 1.** Homology models of *D. mawsoni*  $\gamma$ S1- (gray) and  $\gamma$ S2-crystallin (blue) based upon the solution NMR structure of human  $\gamma$ S-crystallin.

hγS	1	-----GSKTGTKITFYEDKNFQGRYDCDCADFHLYLSCNSIKVEGGTWAIVYERPNFAGMYILPQGEYPEYQR-WMGLNDRL	80
TγS1	1	-----GSSKITFYEDRNFQGRSHECTDCPDHHPFRCNSIKVESGCWVLYERPNYTGQYVLTARGEYPDYQR-WMGFNDSI	77
TγS2	1	-----GKIAFFEDKNFQGRSHECTDCPDLSYFRCNSIKVESGCWVLYERPNYTGQYVLTARGEYPDHQQ-WMGFNDSI	74
DγB	1	-----KLAKNMDRMGKIVFYEDRNFQGRSECSLDCELSHFTRCNSIRVENGAWVLYERPNYMGFYILTARGEYPDYQR-WMGYNDTI	84
DγS3	1	RLTEAIFSEPRPISLKIVFYEDRNFQGRSECSLDCELSHFTRCNSIRVENGAWVLYERPNYMGFYILTARGEYPDYQR-WMGYNDTI	89
cLyS1	1	-----GKVTIFYEDRNFQGRSECTDCSDMHSYLRCHSCRVESGCWVLYDRNFMGNQYFMRRGEYADYMSMWGWNCCI	76
cLyS2	1	-----GKVIIFYEDRNFQGRSECTDCSDMHSYLRCHSCRVESGCWVLYDRNFMGNQYFIRRGGEYADYMSMWGWNCCI	76
chγS1	1	-----GKIIFYEDRNFQGRHYECSSDCADLSPYFSRCNSIRVESDWWVLYERPNYMGYQVLTARGEYPDYQR-WMGFNDCV	75
chγS2	1	-----GKIIFYEDRNFQGRHYECSSDCADLSPYFSRCNSIRVESDWWVLYERPNYMGYQVLTARGEYPDYQR-WMGFNDCV	75
hγS	81	SSCRAVHLPSGGQYKIQIFEKGFDSGQ-MYETTEDCPSIMEQFHMREIHSCKVLEGVWIFYPNLYRGRQYLLDKKEYRKPIDWGAASP	168
TγS1	78	RSCRTFSYTSSEGPYRMRIYERPNFQGG-MMEFSDCESVQENFCSH-DIYSCNVMEGYWTLYEQPNYRGRQYFMRPGEYRKFSFDWGATCA	165
TγS2	75	KSCRSIQNVYKSKWKIRFYENKDFEQG-AAECVEDCASVYETFKFQ-EVHSSVMDGAWVLYEQPNYCGHQYFLEKGEYNNYTDWGATSP	164
DγB	85	RSCRMVRN-HTGSFRIRLYERPDFFQGG-TMESSDWPISLYDRFRQR-EVHSCNVLDGAWIFFEHPNYRGRQYLLKGEYRCFTDWNAMHP	171
DγS3	90	RSCRMVRN-HTGSFRIRLYERPDFFQGG-TMESSDWPISLYDRFRQR-EVHSCNVLDGAWIFFEHPNYRGRQYLLKGEYRCFTDWNAMHP	176
cLyS1	77	RSCRMIPM-YKGSYRMKVYERENFNQSRQMDVMDCCDSFMDRYHWSNSFMSCNVMDAHWLMYEHPHYRGRMWYFRPGEYRNFRDYGGMR-	164
cLyS2	77	RSCRMIPM-YRGAYRMKIYERENFLQG-MMEISDDCDSIMDRYRWSGGCHSCHVTGGHWMYEPHYRGRMWYFRPGEYRSFRDFGNTN-	163
chγS1	76	RSCRMIPH-TGRSYRMRIYERLTFGGQ-MMEIMDDCPSVYDRFRYR-DIHSQVMDGYWIFFEHPNYRGRQYFMRPGEYRYSYDWGGYSS	162
chγS2	76	RSCRVPTH-TQRPYRMRIYERPDFFQGG-MMEFMDVCPVYDRFRYR-DIHSQVMDGYWIFFEHPNYRGRQYFMRPGEYRYSYDWGGYSS	162
hγS	169	AVQSFRRIVE-178	
TγS1	166	TGTSFRRITEF-176	
TγS2	165	AVGSFRRMITKF-175	
DγB	172	TVGSIRRIQDF-182	
DγS3	177	TVGSIRRIQDF-187	
cLyS1	165	-FMSMRMVA-173	
cLyS2	164	-FMSMRIMA-172	
chγS1	163	TVGSLRRIME-172	
chγS2	163	TIGSFRRIME-172	

**Figure 2.** Sequence alignment of human  $\gamma$ S-crystallin (h $\gamma$ S), *D. mawsoni*  $\gamma$ S1- and  $\gamma$ S2-crystallin (T $\gamma$ S1 and T $\gamma$ S2), *D. rerio*  $\gamma$ SB- (D $\gamma$ B) and  $\gamma$ S3-crystallin (D $\gamma$ S3), *C. fuscus*  $\gamma$ S1- and  $\gamma$ S2-crystallin (cLyS1 and cLyS2), and *C. indicum*  $\gamma$ S1- and  $\gamma$ S2-crystallin (ch $\gamma$ S1 and ch $\gamma$ S2). *D. mawsoni*  $\gamma$ S1 and  $\gamma$ S2 have overall sequence identities of 57% and 53% with  $\gamma$ S-crystallin, respectively, and 60% sequence identity to one another. Many residues are conserved among all the  $\gamma$ -crystallins shown. The residues are colored according to their chemical properties as follows: green, hydrophobic residues (AVFPMILW); blue, acidic residues (DE); magenta, basic residues (RK); black, all other residues (STYHCNGQ).

Urea stock solutions were prepared as outlined by Pace et al.<sup>32</sup> Samples were allowed to equilibrate for at least 24 h before absorption–emission fluorescence spectra were obtained using a F4500 fluorescence spectrophotometer (Hitachi, Tokyo, Japan) with a  $\lambda_{\text{ex}}$  of 280 nm. The ratio of baseline-corrected emission intensities at 360 and 320 nm was used for analysis. To determine the thermodynamic parameters ( $\Delta G_w^\circ$  and  $m$  values),  $\Delta G_{[\text{urea}]}$  was calculated from the normalized equilibrium unfolding data and a linear least-squares fit was performed in Mathematica to the line

$$\Delta G_w^\circ = m[\text{urea}] \quad (1)$$

where  $\Delta G_w^\circ$  is the value of  $\Delta G$  at 25 °C, extrapolated to zero concentration of denaturant, and  $m$  is a measure of the dependence of  $\Delta G$  on denaturant concentration.

**Dynamic Light Scattering.** Dynamic light scattering (DLS) measurements were obtained with a Zetasizer Nano

ZS (Malvern Instruments, Malvern, U.K.) on  $\gamma$ S1 and  $\gamma$ S2 at a concentration of 1.0 mg·mL<sup>−1</sup> in 10 mM phosphate buffer, pH 6.9. At each temperature, the sample was allowed to equilibrate for 2 min before measurements were obtained, after which scattering measurements were performed in triplicate, resulting in a heating rate of  $\sim 0.5$  °C·min<sup>−1</sup>.

**Transmittance.** Transmittance was obtained using a Cary 4000 UV–vis (Agilent Technologies, Santa Clara, U.S.) on h $\gamma$ S, T $\gamma$ S1, and T $\gamma$ S2 at a concentration of 10.0 mg·mL<sup>−1</sup> in 10 mM phosphate buffer, pH 6.9, from 25 to 5 °C.

## RESULTS AND DISCUSSION

**Primary Sequence Analysis Suggests Adaptation for High Refractivity.** The structural  $\beta\gamma$ -crystallins share a common fold consisting of paired homologous double Greek key domains, each with two sets of four adjacent antiparallel  $\beta$ -strands linked by short loops. This protein architecture has



Table 1. Refractive Index Increment by Amino Acid Type

amino acid type	dn/dc from ref 11 (mL/g)	frequency, average (%)	frequency, hγS human (%)	frequency, TγS1 toothfish (%)	frequency, TγS2 toothfish (%)	frequency, DγB zebrafish (%)	frequency, DγS3 zebrafish (%)	frequency, chγS1 shark (%)	frequency, chγS2 shark (%)	frequency, cLγS1 catfish (%)	frequency, cLγS2 catfish (%)
Ala (A)	0.167	7.4	3.9	1.1	4.0	2.2	2.1	0.6	1.2	1.7	1.7
Arg (R)	0.206	4.3	7.3	9.1	4.6	12.1	12.3	12.8	12.8	12.1	12.2
Asn (N)	0.192	4.4	2.8	4.5	5.7	5.5	4.8	2.9	3.5	5.8	4.7
Asp (D)	0.197	5.9	5.6	5.1	5.2	6.0	5.3	7.0	6.4	6.9	5.8
Cys (C)	0.206	3.3	3.9	5.1	5.2	3.3	3.2	4.1	3.5	5.2	5.8
Gln (Q)	0.186	3.7	5.1	4.5	5.2	4.4	4.3	3.5	2.9	1.2	1.7
Glu (E)	0.183	5.8	7.9	8.5	8.0	7.1	8.0	5.8	5.8	4.6	4.7
Gly (G)	0.175	7.4	8.4	6.8	7.5	6.6	5.9	8.1	7.6	8.1	9.9
His (H)	0.219	2.9	2.2	2.3	2.3	2.7	2.7	2.3	2.9	3.5	2.9
Ile (I)	0.179	3.8	5.6	3.4	3.4	4.4	5.3	4.7	4.7	1.2	4.7
Leu (L)	0.173	7.6	5.1	1.7	2.9	5.5	5.9	3.5	2.3	0.6	1.7
Lys (K)	0.181	7.2	5.6	2.3	5.2	2.2	1.1	1.2	1.2	1.7	1.7
Met (M)	0.204	1.8	2.8	4.5	2.3	3.8	2.7	5.8	5.2	12.7	9.3
Phe (F)	0.244	4.0	5.1	6.8	6.9	6.6	7.0	4.7	5.8	5.8	5.8
Pro (P)	0.165	5.0	4.5	4.5	2.9	3.8	4.8	4.1	5.2	1.7	2.9
Ser (S)	0.170	8.1	6.2	8.5	8.6	6.6	7.5	8.1	8.1	8.7	9.3
Thr (T)	0.172	6.2	3.9	6.8	3.4	3.8	4.3	2.3	2.3	1.7	1.2
Trp (W)	0.277	1.3	2.2	2.3	2.9	2.7	2.7	2.9	2.9	3.5	3.5
Tyr (Y)	0.240	3.3	7.9	9.1	7.5	6.6	6.4	11.6	11.0	9.2	8.1
Val (V)	0.172	6.8	3.9	2.8	6.3	3.8	3.7	4.1	4.7	4.0	2.3

Table 2. Sequence Analysis of Selected γS-Crystallins

	GRAVY	aliphatic index	no. of −ve charged residues	no. of +ve charged residues	predicted dn/dc (ref 11)	predicted pI	charge, neutral pH
hγS	−0.685	56.97	24	23	0.1983	6.4	−0.9
TγS1	−0.957	29.32	24	20	0.2020	5.6	−4.0
TγS2	−0.651	47.01	23	17	0.2002	5.2	−6.0
DγB	−0.855	51.92	24	26	0.2013	8.3	2.2
DγS3	−0.779	56.79	25	25	0.2006	7.1	0.2
chγS1	−0.858	44.13	22	24	0.2044	8.2	2.1
chγS2	−0.867	41.86	21	24	0.2046	8.5	3.2
cLγS1	−0.857	20.23	20	24	0.2071	8.6	4.1
cLγS2	−0.717	33.43	18	24	0.2053	8.8	6.0

been identified as contributing to the very high stability of the βγ-crystallins,<sup>33</sup> particularly the tight interdomain interface that contains several critical hydrophobic interactions.<sup>34</sup> Homology models for Tγ1 and TγS2 based on the solution structure of hγS (PDB code 2M3T)<sup>35</sup> were constructed using SwissModel.<sup>36</sup> and are shown in Figure 1.

The primary sequence of γS-crystallin is highly conserved across diverse species including fish, mammals, and birds.<sup>37–40</sup> A sequence alignment for hγS, TγS1, TγS2, and a selection of their orthologs from other fish species is shown in Figure 2. Both TγS1 and TγS2 have moderate sequence identity to hγS (57% and 53%, respectively). Conserved residues include the four tryptophans, several glycines in loops, and other structurally important residues. A BLAST search<sup>41</sup> reveals many other homologues from mesophilic fish species; here we examine some examples from classes Chondrichthyes (cartilaginous fish, such as sharks and rays) and Osteichthyes (teleost fish, which includes *D. mawsoni*, and the well-known model organism *Danio rerio*). Although other putative sequences identified from DNA open reading frames were more closely related in some cases, our analysis is limited to a selection of sequences confirmed from mRNA transcripts. The sequences whose properties are summarized in Table 1 include the zebrafish (*Danio rerio*) γB-crystallin (DγB)<sup>42</sup> and γS3-crystallin

(DγS3),<sup>43</sup> the Chinese catfish (*Clarias fuscus*) γS1- and γS2-crystallins (cLγS1 and cLγS2),<sup>44</sup> and the slender bamboo shark (*Chiloscyllium indicum*) γS1- and γS2-crystallin (chγS1 and chγS2).<sup>45</sup>

In general, the amino acid composition of proteins is relatively constant, as it primarily depends on factors such as the codon redundancy and mutation tolerance,<sup>46,47</sup> such that deviation from the average amino acid frequency is often indicative of selection for a particular function or environmental adaptation. For example, thermophilic proteins are often enriched in arginine because of its importance in forming stabilizing salt bridges.<sup>48</sup> Many psychrophilic proteins are exiguous in proline content.<sup>30,49</sup> Eye lens proteins, which have been selected for their high refractive index increments, are enriched in highly polarizable amino acids such as Trp, Tyr, Phe, Arg, Met, and Cys and exiguous in aliphatic residues.<sup>12</sup> The amino acid frequencies for hγS, TγS1, TγS2, and the other fish γ-crystallins described above are given in Table 1 along with the average values for vertebrate proteins and the contribution of each amino acid type to dn/dc.

The grand average of hydropathicity index (GRAVY) predicts the hydrophobic character of the proteins where more positive values indicate higher hydrophobicity.<sup>50</sup> Table 2 summarizes the sequence characteristics of hγS, TγS1, TγS2,

and several homologous proteins from mesophilic fish, as calculated from the ExPASy ProtParam tool.<sup>51</sup> The aliphatic index measures the relative volume occupied by aliphatic side chains (nonpolar, hydrophobic) including alanine, valine, isoleucine, and leucine.<sup>52</sup> All of the  $\gamma$ -crystallins investigated here are moderately hydrophilic, with small negative GRAVY values. T $\gamma$ S2 is the most hydrophobic of the proteins studied, yet it has a lower aliphatic index than h $\gamma$ S, reflecting its enhanced content of aromatic residues. h $\gamma$ S has the next most positive GRAVY value and the highest aliphatic character, along with both zebrafish proteins. The toothfish  $\gamma$ S1 and both catfish proteins have the least aliphatic character. Thus, in terms of GRAVY index and aliphatic character, the toothfish crystallins are within the range of variance established by the comparison group of mesophilic fish sequences. Selection for cold tolerance often leads to decreased numbers of hydrophobic residues in the protein core, and more on the surface,<sup>53</sup> reflecting the reduced entropy cost of exposing hydrophobic groups to solvent at low temperatures. A large proteomic analysis of the amino acid composition of psychrophilic and mesophilic proteins found that psychrophilic proteins have a larger number of hydrophobic residues in loops and a smaller number in helices, relative to their mesophilic counterparts.<sup>54</sup> This was consistent with the well-known idea that aliphatic amino acids in the core of the protein contribute to stability via the hydrophobic effect.<sup>55</sup>

Some sequence commonalities can be observed among all the fish  $\gamma$ S-crystallins investigated here, due to their both their common ancestry and the selective pressures on lens proteins. In general, alanine, valine, isoleucine, and leucine are expected to be selected against in lens proteins because these amino acids have low refractive index increments. As expected based on the requirement for higher refractivity in the lenses of aquatic organisms, all of the fish crystallins have higher predicted  $dn/dc$  values than h $\gamma$ S. Consistent with this idea, T $\gamma$ S1 has the lowest aliphatic index, as well as a higher predicted  $dn/dc$  than h $\gamma$ S. Selection for increased refractive index leads to reduced fraction of aliphatic residues in favor of those with more polarizable side chains.<sup>11,12</sup> This would lead to the expectation that the  $\gamma$ S-crystallins would have an unusually high proportion of the aromatic amino acids Phe, Tyr, and Trp to compensate, which is the case for all of the proteins listed in Table 1. For example, toothfish  $\gamma$ S1, which has the highest predicted  $dn/dc$ , has 9.1% Tyr, almost 3 times the average value, and is also enriched in Phe (6.8% vs the average of 4.0%).

Other highly polarizable residues that would be expected to be enriched in lens proteins include Arg, Met, Cys, and His. Methionine in particular has been cited as being particularly important in providing the high refractivity required for fish crystallins, as it is greatly enriched in the abundant  $\gamma$ M-crystallin of the zebrafish lens.<sup>18</sup> Although all the proteins have a Met content greater than its average value of 1.8%, the level of enrichment varies greatly: the catfish proteins cL $\gamma$ S1 and cL $\gamma$ S2 have the highest Met content (12.7% and 9.3%, respectively), while the other crystallins have more moderate levels of enrichment ranging from 2.3% to 5.8%, with T $\gamma$ S1 and T $\gamma$ S2 falling within this range. The situation for His and Cys is comparable; all of the crystallins studied have His contents close to the average value, while Cys levels are slightly elevated for the toothfish crystallins but also for the catfish proteins. The major difference between the toothfish crystallins and their mesophilic homologues is in their Arg content. Arg is often exiguous in cold-adapted proteins because of its role in the

formation of stabilizing salt bridges. In this case, all the  $\gamma$ -crystallins investigated are significantly enriched in Arg except for T $\gamma$ S2, which has approximately the average value. The next lowest Arg content values are found in h $\gamma$ S and T $\gamma$ S1. The relative amounts of Arg in the two *D. mawsoni* crystallins may provide insight into their denaturation behavior, which is described in the next section. Taken together, these observations suggest that rather than any one residue being critical for determining the high  $dn/dc$  values required for function in fish lens proteins, this function can be acquired by different combinations of high-refractivity amino acids, within the constraints imposed by the additional selection for cold tolerance in the *D. mawsoni* proteins.

The toothfish crystallins have lower isoelectric point (pI) values with respect to h $\gamma$ S, meaning that they have much more negative charge at neutral pH. This is consistent with the previous observation that psychrophilic proteins often have more acidic pI values than homologous mesophilic or thermophilic proteins, possibly because negatively charged residues are important for mediating interactions with the solvent and hence maintaining flexibility in cold environments.<sup>26</sup> Alternatively, in this case it may simply reflect the reduction in positive charge due to the decreased arginine content of T $\gamma$ S1 and T $\gamma$ S2 relative to the  $\gamma$ S-crystallins from mesophilic fish.

**T $\gamma$ S1 and T $\gamma$ S2 Are Both Folded, with Primarily  $\beta$ -Sheet Secondary Structure.** By use of PsiPred, a secondary structure prediction software,<sup>56,57</sup> the sequences for both T $\gamma$ S1 and T $\gamma$ S2 were predicted to have primarily  $\beta$ -sheet secondary structures. The prediction results are shown in Figure 3.

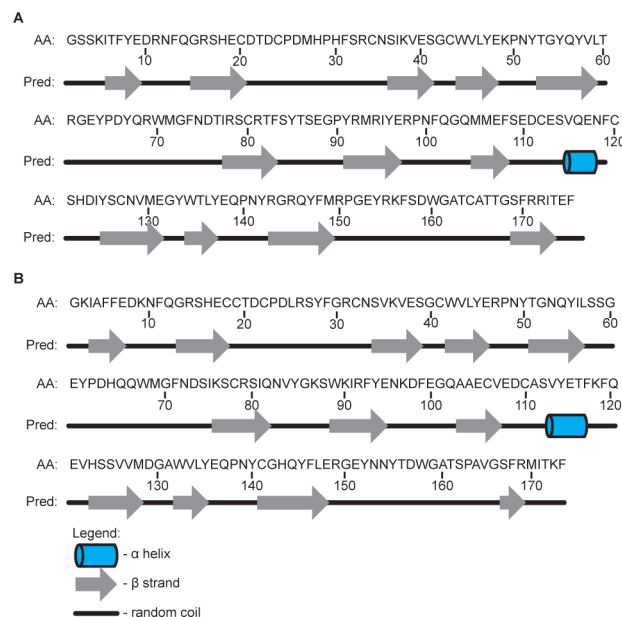


**Figure 3.** Predicted secondary structures of *D. mawsoni* (A)  $\gamma$ S1 and (B)  $\gamma$ S2.

Circular dichroism (CD) spectra were collected for both T $\gamma$ S1 and T $\gamma$ S2 to assess the overall general secondary structures of the proteins (Figure 4). A comparison of the circular dichroism spectra of T $\gamma$ S1 and T $\gamma$ S2 at 25 °C indicates that both proteins have primarily  $\beta$ -sheet secondary structures. The negative ellipticities of T $\gamma$ S1 and T $\gamma$ S2 occur at 216 and 217 nm, respectively. These values are in the range that is

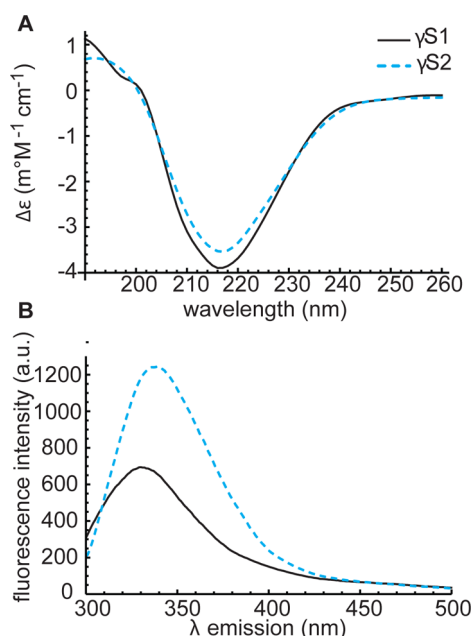


**Figure 4.** (A) Circular dichroism spectra of *D. mawsoni*  $\gamma$ S1- and  $\gamma$ S2-crystallins.  $\gamma$ S1 displays a negative ellipticity at 216 nm, while  $\gamma$ S2 displays a negative ellipticity at 217 nm. Both of these values are indicative of primarily  $\beta$ -sheet secondary structures. (B) Tryptophan fluorescence emission spectra of T $\gamma$ S1 and T $\gamma$ S2. T $\gamma$ S1 has an emission maximum at 331 nm, and the emission maximum for T $\gamma$ S2 is 336 nm.

typical of  $\beta$ -sheet proteins and is consistent with the predicted secondary structure results and with the experimental results for h $\gamma$ S.<sup>58</sup>

The intrinsic fluorescence of crystallin proteins is an important indication of the degree of folded structure in the double Greek key domains, as the fluorescence is primarily due to four highly conserved tryptophan residues in the protein core. Both T $\gamma$ S1 and T $\gamma$ S2 share these conserved tryptophans; T $\gamma$ S2 also has a fifth tryptophan. In mammalian eye lenses, the positioning of the conserved tryptophan side chains is essential for the rapid quenching of UV fluorescence hypothesized to protect crystallins from photochemical degradation in species that are subject to strong UV light exposure.<sup>59</sup> Their conservation in this aquatic species may be due to their contributions to the  $dn/dc$ , hydrophobic packing, or both. UV fluorescence spectra for *D. mawsoni*  $\gamma$ S1 and  $\gamma$ S2 are shown in Figure 4. The emission maxima in the fluorescence spectra for excitation at 280 nm are 331 and 336 nm for T $\gamma$ S1 and T $\gamma$ S2, respectively. T $\gamma$ S2 has increased fluorescence intensity in comparison to T $\gamma$ S1 due to the presence of the additional tryptophan in its sequence. The reported  $\lambda_{\max}$  for tryptophan fluorescence of h $\gamma$ S is 326 nm.<sup>58</sup> Typically, tryptophan fluorescence emission maxima are in the range of 300–350 nm. Tryptophans that are exposed to water have emission maxima between 340 and 350 nm, whereas completely buried tryptophans have maxima around 330 nm. The slight red shifts of both T $\gamma$ S1 and T $\gamma$ S2 with respect to h $\gamma$ S indicate that the tryptophans in both toothfish proteins are more exposed to water, suggesting that T $\gamma$ S1 and T $\gamma$ S2 are less compactly folded and more structurally flexible than h $\gamma$ S, as expected.

Cold denaturation, protein unfolding due to the decreased energetic cost of exposing hydrophobic residues to solvent, does not occur for most globular proteins until well below the

freezing point of water. Except in special cases, experimental studies of cold denaturation have required the use of chemical denaturants, high pressure,<sup>60</sup> encapsulation in reverse micelles,<sup>61</sup> or limiting the sample volume to small capillaries<sup>62</sup> to study the unfolding intermediates. Thus, cold cataract, the low-temperature opacity of many protein solutions such as mammalian lenses, results from liquid–liquid phase separation rather than protein unfolding. The toothfish eye lens does not undergo cold cataract above its freezing point of  $-12\text{ }^{\circ}\text{C}$ , in contrast to mammalian lenses, which form them at much higher temperatures ( $\sim 20\text{ }^{\circ}\text{C}$ ).<sup>25</sup>  $\gamma$ S-Crystallins in general are resistant to cold cataract and are thought to play an important role in maintaining solubility in multicomponent crystallin mixtures; e.g., bovine  $\gamma$ S-crystallin has a theoretical liquid–liquid phase separation temperature of  $-28\text{ }^{\circ}\text{C}$ <sup>63</sup> and its presence in concentrated solutions of other  $\gamma$ -crystallins results in a lowered phase separation temperature.<sup>64</sup> Transmission measurements at 600 nm were taken as a function of temperature in order to establish that solutions of our in vitro generated protein constructs are transparent over the experimentally relevant temperature range (i.e., cold cataract does not occur). These results, summarized in Table 3, indicate that h $\gamma$ S,  $\gamma$ S1, and  $\gamma$ S2

**Table 3.** Transmittance of h $\gamma$ S, T $\gamma$ S1, and T $\gamma$ S2 from 25 to 5  $^{\circ}\text{C}$

temp ( $^{\circ}\text{C}$ )	transmittance ( $\lambda = 600\text{ nm}$ )		
	h $\gamma$ S	T $\gamma$ S1	T $\gamma$ S2
25	0.93	0.98	0.97
20	0.95	0.93	0.97
15	0.95	0.91	0.97
10	0.94	0.88	0.97
5	0.93	0.87	0.97

all remain transparent at 5  $^{\circ}\text{C}$ , consistent with previous measurements of  $\gamma$ S-crystallins. Although solutions of each of the  $\gamma$ -crystallins studied here remain transparent at 5  $^{\circ}\text{C}$ , further investigations will be needed to assess their ability to stabilize mixtures of other crystallins as a function of temperature. Enhanced low-temperature stability has been previously observed in cold-adapted teleost  $\alpha$ A-crystallins, which have greater hydrophobic character and are better able to maintain their chaperone activity at lower temperatures than their mesophilic orthologs at the cost of high thermal stability.<sup>65</sup>

**$\gamma$ S1 and  $\gamma$ S2 Have Different Relative Stabilities under Chemical and Thermal Denaturation.** The overall thermodynamic stability of the  $\gamma$ S-crystallin fold is highly relevant to the biological function of the eye lens because of the lack of protein turnover in the lens; the crystallins must remain stable and soluble for decades. In general, cold-stable proteins are generally more susceptible to chemical denaturation than their higher-temperature counterparts.<sup>30</sup> Factors affecting overall protein stability include hydrophobic interactions, hydrogen bonds, and conformational entropy.

T $\gamma$ S1 and T $\gamma$ S2 were subjected to chemical denaturation with increasing concentrations of urea, while fluorescence spectroscopy was used to monitor unfolding. Each sample was allowed to equilibrate for at least 24 h before fluorescence measurements were collected. The excitation wavelength was 280 nm, and emission spectra were collected between 300 and 500 nm. Fluorescence maximum intensities were normalized by taking the F360/320 ratio at each concentration of denaturant and plotted as fraction unfolded vs denaturant concentration

(Figure 5A). The data points indicated with open circles in Figure 5A represent dilution of the samples to 2 M urea after

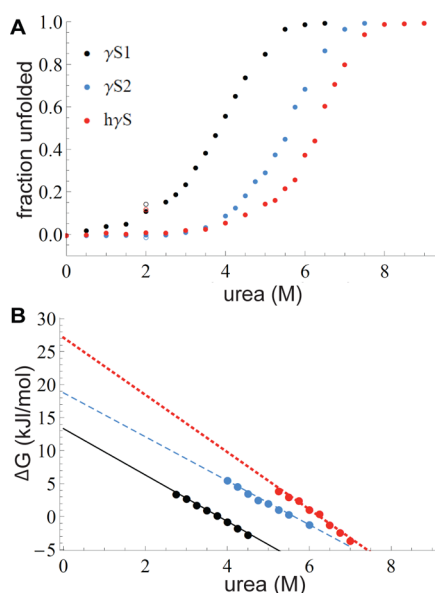


**Figure 5.** (A) Chemical denaturation curves of h $\gamma$ S, *D. mawsoni*  $\gamma$ S1 and  $\gamma$ S2 with varying amounts of urea, measured by fluorescence spectroscopy and plotted as fraction unfolded. All three proteins exhibit two-state equilibrium unfolding behavior by urea denaturation. Data points designated with open circles represent samples of h $\gamma$ S, T $\gamma$ S1, and T $\gamma$ S2 that were first unfolded with 7 M urea and then diluted to 2 M urea to indicate that urea denaturation is reversible. (B)  $\Delta G$  vs denaturant concentration for the transition regions of the chemical unfolding curves used to extrapolate values for  $\Delta G(\text{H}_2\text{O})$ .  $\gamma$ S1 is more susceptible to unfolding by urea at lower concentrations where  $\Delta G(\text{H}_2\text{O})$  is 13.35 and 18.74 kJ·mol<sup>-1</sup> for  $\gamma$ S1 and  $\gamma$ S2, respectively.

full unfolding at 7 M urea, demonstrating the reversibility of this transition. Figure 5B is a plot of  $\Delta G$  vs denaturant concentration for the transition regions of the unfolding curves used to extrapolate values for  $\Delta G_w^\circ$ , the  $\Delta G$  at 25 °C in the absence of any denaturant.<sup>32</sup> T $\gamma$ S1 is more susceptible to unfolding by urea; the  $[\text{urea}]_{1/2}$  of  $\gamma$ S1 is equal to 3.8 and 5.6 M for T $\gamma$ S2.  $\Delta G_w^\circ$  is 13.35 and 18.74 kJ mol<sup>-1</sup> for T $\gamma$ S1 and T $\gamma$ S2, respectively. The thermodynamic parameters calculated from these denaturation curves are summarized in Table 4. Urea

**Table 4. Thermodynamic Parameters from Chemical Denaturation of T $\gamma$ S1 and T $\gamma$ S2**

	T $\gamma$ S1	T $\gamma$ S2	h $\gamma$ S
$[\text{urea}]_{1/2}$ (M)	3.8	5.6	6.3
$\Delta G_w^\circ$ (kJ·mol <sup>-1</sup> )	13.35	18.74	27.12
$m$ (kJ·mol <sup>-1</sup> M <sup>-1</sup> )	3.51	3.35	4.33
$T_m$ (°C)	68.5 $\pm$ 0.1	58.0 $\pm$ 0.1	72.0 $\pm$ 0.1 <sup>58</sup>

unfolding is thought to be driven by a combination of indirect and direct mechanisms.<sup>66</sup> It weakens the hydrophobic effect by disrupting the hydrogen bonding network of the solvent, as well as stabilizing unfolded states via direct electrostatic and hydrogen bonding interactions with side chain and backbone groups.<sup>67–69</sup> More urea may be needed to unfold T $\gamma$ S2 because it has nearly twice as many aliphatic residues as T $\gamma$ S1 and fewer hydrophilic amino acid residues. The slope,  $m$ , describing the

dependence of  $\Delta G$  on denaturant concentration, is very similar for both T $\gamma$ S1 and T $\gamma$ S2.

Thermal denaturation provides complementary information regarding protein stability and aggregation propensity. For some proteins, e.g., lysozyme,<sup>70</sup> the thermally denatured state has been shown to differ from that induced by chemical denaturation. Furthermore, this process is often irreversible, making the calculation of thermodynamic quantities problematic; however, the midpoint of the unfolding transition ( $T_m$ ) is itself a useful measure of protein stability. The thermal denaturation of T $\gamma$ S1 and T $\gamma$ S2 was monitored by circular dichroism at 218 nm (Figure 6) and fit to a two-state

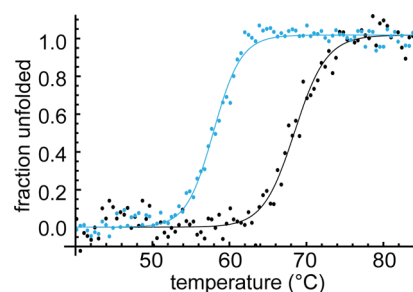


**Figure 6.** Thermal unfolding curves of T $\gamma$ S1 and T $\gamma$ S2 measured by monitoring the circular dichroism signal at 218 nm, with best-fit unfolding curves.  $T_m$  values for T $\gamma$ S1 and T $\gamma$ S2 are 68.5 and 58.0 °C, respectively. Both proteins exhibit two-state equilibrium unfolding behavior.

equilibrium unfolding model. The CD melting curves obtained provide information about the overall stability of the protein folds. The difference in thermal stabilities between the two proteins is quite different; T $\gamma$ S1 has a  $T_m$  of 68.5  $\pm$  0.1 °C, while T $\gamma$ S2 had a  $T_m$  of 58.0  $\pm$  0.1 °C. For comparison, human  $\gamma$ S-crystallin has a  $T_m$  of 72.0  $\pm$  0.1 °C under the same conditions.<sup>58</sup> The relationship between thermal stability, hydrophobicity, and aliphatic index is not immediately clear for these proteins; T $\gamma$ S2, the most hydrophobic crystallin studied, has the lowest  $T_m$  while  $\gamma$ S1, the least hydrophobic, does not have the highest  $T_m$  value. The highest  $T_m$  belongs to h $\gamma$ S, which has a hydrophobic content between those of T $\gamma$ S1 and T $\gamma$ S2. The explanation for this surprising observation may be a result of selection for high  $dn/dc$ . T $\gamma$ S1, but not T $\gamma$ S2, is enriched in Arg, which is known for increasing stability in thermophilic proteins, due to the ability of the guanidinium group to form stabilizing salt bridges. Although increased arginine content should stabilize the protein with respect to thermal denaturation, as seen for h $\gamma$ S and T $\gamma$ S1, chemical denaturation by urea should affect these salt bridges the same way as any other polar interaction, meaning that other factors such as hydrophobicity come into play in T $\gamma$ S2.

Aggregation under thermal stress was also measured as a function of temperature using dynamic light scattering (DLS) for both toothfish  $\gamma$ S-crystallins to ascertain their aggregation propensity. Aggregation propensity is not always directly correlated with thermal stability.<sup>58</sup> At even moderately high concentrations, protein aggregates can form well below the thermal denaturation temperature as a result of interactions between transiently exposed groups in conformationally mobile protein monomers. The measurements were made in 10 mM phosphate buffer with no additional reducing agents to avoid interfering with any attractive intermolecular forces that may be responsible for aggregation. For each data point, taken in



triplicate, the sample was allowed to equilibrate for 2 min prior to measurement at a given temperature. Three scans of % abundance by number were averaged at each temperature and then fit to a Gaussian function using nonlinear regression. The average apparent particle size is plotted as a function of temperature in Figure 7. T $\gamma$ S1 remains monomeric until 35.0 °C

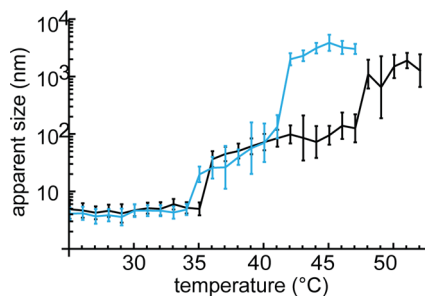


**Figure 7.** DLS measurements of thermally induced aggregation of T $\gamma$ S1 and T $\gamma$ S2. T $\gamma$ S1 is monomeric until 35.0 °C where it begins to form intermediate aggregates and then finally to form large aggregates around 48.0 °C. T $\gamma$ S2 behaves similarly, but because it is not as thermally stable, it forms intermediate sized aggregates at 34.0 °C and large aggregates 42.0 °C.

°C where intermediate aggregates in the range 30–100 nm begin to form before quickly transitioning into larger aggregates up to 1200 nm in size at 47.5 °C. T $\gamma$ S2 follows a similar trend, but intermediate sized aggregates begin forming at 34.0 °C and large aggregates at 42.0 °C. In comparison, intermediate aggregates of h $\gamma$ S do not begin forming until around 49.0 °C while larger aggregates appear at 58.5 °C.<sup>58</sup> Both T $\gamma$ S1 and T $\gamma$ S2 are less thermally stable and more aggregation prone than h $\gamma$ S.

In summary, the biophysical characterization of T $\gamma$ S1 and T $\gamma$ S2 showed that while both proteins have the primarily  $\beta$ -sheet secondary structures characteristic of  $\gamma$ -crystallins, they appear to have slightly less overall  $\beta$ -sheet character than their human homologue. T $\gamma$ S1 and T $\gamma$ S2 also appear to have greater structural flexibility as observed in the red-shifted tryptophan fluorescence spectra, indicating that the structurally conserved tryptophans in the core of both proteins are more accessible to water. Of the two crystallins, the less structurally rigid T $\gamma$ S2 has the lowest thermal stability as determined by thermal denaturation despite having a higher  $\Delta G_w$ . Nevertheless, both toothfish crystallins have lower thermal stabilities than h $\gamma$ S and begin forming high molecular weight aggregates at lower temperatures. The biophysical characterization of the *D. mawsoni*  $\gamma$ S1- and  $\gamma$ S2-crystallins demonstrates an unusual set of protein homologues in which thermal stability does not directly correlate with  $\Delta G^\circ$ , and provides a useful model system for future structural and mutagenesis studies pinpointing the molecular determinants of protein solubility, thermal stability, and denaturation resistance.

## AUTHOR INFORMATION

### Corresponding Author

\*E-mail: rwmartin@uci.edu.

### Notes

The authors declare no competing financial interest.

## ACKNOWLEDGMENTS

The authors thank Dmitry Fishman for excellent management of the UCI Optical Spectroscopy Facility. V.P. acknowledges support from the UCI UROP program. This work was supported by NIH Grant R01EY021514 and NSF DMR Grant 1410415 to R.W.M.

## REFERENCES

- (1) Teilum, K.; Olsen, B. B.; Kragelund, B. B. Protein stability, flexibility and function. *Biochim. Biophys. Acta* **2011**, *1814*, 969–976.
- (2) Jaenicke, R.; G. Bohm, G. The stability of proteins in extreme environments. *Curr. Opin. Struct. Biol.* **1998**, *8*, 738–748.
- (3) Land, M. F.; Nilsson, D. E. *Animal Eyes*, 2nd ed.; Oxford Animal Biology; Oxford University Press (Great Clarendon St., Oxford OX2 6DF), 2012.
- (4) Delaye, M.; Tardieu, A. Short-range order of crystallin proteins accounts for eye lens transparency. *Nature* **1983**, *302*, 425–417.
- (5) Kroger, R. H.; Campbell, M. C.; Munger, R.; Fernald, R. D. Refractive index distribution and spherical aberration in the crystalline lens of the African cichlid fish *Haplochromis burtoni*. *Vision Research* **1994**, *34*, 1815–1822.
- (6) Horwitz, J. Alpha-crystallin can function as a molecular chaperone. *Proc. Natl. Acad. Sci. U.S.A.* **1992**, *89*, 10449–10453.
- (7) Slingsby, C.; Wistow, G. J.; Clark, A. R. Evolution of crystallins for a role in the vertebrate eye lens. *Protein Sci.* **2013**, *22*, 367–380.
- (8) Ingolia, T.; Craig, E. Four small *Drosophila* heat shock proteins are related to each other and to mammalian alpha-crystallins. *Proc. Natl. Acad. Sci. U.S.A.* **1982**, *79*, 2360–2364.
- (9) de Jong, W. W.; Leunissen, J. A. M.; Voorter, C. E. M. Evolution of the alpha-crystallin/small heat shock protein family. *Mol. Biol. Evol.* **1993**, *10*, 103–126.
- (10) Piatigorsky, J.; Wistow, G. J. Enzyme crystallins—gene sharing as an evolutionary strategy. *Cell* **1989**, *57*, 197–199.
- (11) Zhao, H.; Brown, P. H.; Schuck, P. On the distribution of protein refractive index increments. *Biophys. J.* **2011**, *100*, 2309–2317.
- (12) Zhao, H.; Brown, P. H.; Magone, M. T.; Schuck, P. The molecular refractive function of lens  $\gamma$ -crystallins. *J. Mol. Biol.* **2011**, *411*, 680–699.
- (13) Aravind, P.; Mishra, A.; Suman, S. K.; Jobby, M. K.; Sankaranarayanan, R.; Sharma, Y. The  $\beta\gamma$ -crystallin superfamily contains a universal motif for binding calcium. *Biochemistry* **2009**, *48*, 12180–12190.
- (14) Barnwal, R.; Jobby, M. K.; Devi, K. M.; Sharma, Y.; Chary, K. V. Solution structure and calcium-binding properties of M-crystallin, a primordial betagamma-crystallin from archaea. *J. Mol. Biol.* **2009**, *386*, 675–689.
- (15) Clout, N. J.; Kretschmar, M.; Jaenicke, R.; Slingsby, C. Crystal structure of the calcium-loaded spherulin 3a dimer sheds light on the evolution of the eye lens betagamma-crystallin domain fold. *Structure* **2001**, *9*, 115–124.
- (16) Shimeld, S. M.; Purkiss, A. G.; Dirks, R. P.; Bateman, O. A.; Slingsby, C.; Lubsen, N. H. Urochordate betagamma-crystallin and the evolutionary origin of the vertebrate eye lens. *Curr. Biol.* **2005**, *15*, 1684–1689.
- (17) Suman, S. K.; Mishra, A.; Yeramala, L.; Das Rastogi, I.; Sharma, Y. Disability for function: loss of Ca<sup>2+</sup>-binding is obligatory for fitness of mammalian  $\beta\gamma$ -crystallins. *Biochemistry* **2013**, *52*, 9047–9058.
- (18) Mahler, B.; Chen, Y.; Ford, J.; Thiel, C.; Wistow, G.; Zu, Z. Structure and dynamics of the fish eye lens protein,  $\gamma$ M7-crystallin. *Biochemistry* **2013**, *52*, 3579–3587.
- (19) Posner, M.; Hawke, M.; LaCava, C.; Prince, C. J.; Bellanco, N. R.; Corbin, R. W. A proteome map of the zebrafish (*Danio rerio*) lens reveals similarities between zebrafish and mammalian crystallin expression. *Mol. Vision* **2008**, *14*, 806–814.
- (20) Siezen, R. J.; Fisch, M. R.; Slingsby, C.; Benedek, G. B. Opacification of gamma-crystallin solutions from calf lens in relation to cold cataract formation. *Proc. Natl. Acad. Sci. U.S.A.* **1985**, *82*, 1701–1705.



- (21) Chen, Y.; Zhao, H.; Schuck, P.; Wistow, G. Solution properties of  $\gamma$ -crystallins: compact structure and low frictional ratio are conserved properties of diverse  $\gamma$ -crystallins. *Protein Sci.* **2014**, *23*, 76–87.
- (22) Cantor, C. R.; Schimmel, P. R. *Biophysical Chemistry, Part III: The Behavior of Biological Macromolecules*; W. H. Freeman and Company: New York, 1980.
- (23) Myers, J. K.; Pace, C. N.; Scholtz, J. M. Denaturant  $m$  values and heat capacity changes: relation to changes in accessible surface areas of protein unfolding. *Protein Sci.* **1995**, *4*, 2138–2148.
- (24) Pace, C. N. Conformational stability of globular proteins. *Trends Biochem. Sci.* **1990**, *15*, 14–17.
- (25) Kiss, A. J.; Mirarefi, A. Y.; Ramakrishnan, S.; Zukoski, C. F.; DeVries, A. L.; Cheng, C.-H. C. Cold-stable eye lens crystallins of the Antarctic nototheniid toothfish *Dissostichus mawsoni* Norman. *J. Exp. Biol.* **2004**, *207*, 4633–4649.
- (26) Feller, G.; A'mico, D.; Gerday, C. Thermodynamic stability of a cold-active  $\alpha$ -amylase from the Antarctic bacterium *Alteromonas haloplanctis*. *Biochemistry* **1999**, *38*, 4613–4619.
- (27) Åsgeisson, B.; Hauksson, J. B.; Gunnarsson, H. Dissociation and unfolding of cold-active alkaline phosphatase from atlantic cod in the presence of guanidinium chloride. *Eur. J. Biochem.* **2000**, *267*, 6403–6412.
- (28) D'Amico, S.; Marx, J. C.; Gerday, C.; Feller, G. Activity–stability relationships in extremophilic enzymes. *J. Biol. Chem.* **2003**, *278*, 7891–7896.
- (29) García-Arribas, O.; Mateo, R.; Tomczak, M. M.; Davies, P. L.; Mateu, M. G. Thermodynamic stability of a cold-adapted protein, type III antifreeze protein, an energetic contribution of salt bridges. *Protein Sci.* **2009**, *16*, 227–238.
- (30) Siddiqui, K. S.; Cavicchioli, R. Cold-adapted enzymes. *Annu. Rev. Biochem.* **2006**, *75*, 403–433.
- (31) Kiss, A. J.; Cheng, C.-H. C. Molecular diversity and genomic organisation of the  $\alpha$ ,  $\beta$  and  $\gamma$  eye lens crystallins from the Antarctic toothfish *Dissostichus mawsoni*. *Comp. Biochem. Physiol., Part D* **2008**, *3*, 155–171.
- (32) Pace, C. N.; Scholtz, J. M. Measuring the Conformational Stability of a Protein. In *Protein Structure—A Practical Approach*; Creighton, T. E., Ed.; Oxford University Press, Oxford, U.K., 1997; pp 299–321.
- (33) Macdonald, J. T.; Purkiss, A. G.; Smith, M. A.; Evans, P.; Goodfellow, J. M.; Slingsby, C. Unfolding crystallins: the destabilizing role of a  $\beta$ -hairpin cysteine in  $\beta$  B2-crystallin by simulation and experiment. *Protein Sci.* **2005**, *14*, 1282–1292.
- (34) Mills, I. A.; Flaugh, S. L.; Kosinski-Collins, M. S.; King, J. A. Folding and stability of the isolated Greek key domains of the long-lived human lens proteins  $\gamma$ D-crystallin and  $\gamma$ S-crystallin. *Protein Sci.* **2007**, *16*, 2427–2444.
- (35) Kingsley, C. N.; Brubaker, W. D.; Markovic, S.; Diehl, A.; Brindley, A. J.; Oschkinat, H.; Martin, R. W. Preferential and specific binding of human  $\alpha$ B-crystallin to cataract related variant of  $\gamma$ S-crystallin. *Structure* **2013**, *12*, 2221–2227.
- (36) Guex, N.; Peitsch, M. C. SWISS-MODEL and the Swiss-PdbViewer: an environment for comparative protein modeling. *Electrophoresis* **1997**, *18*, 2714–2723.
- (37) Chang, T.; Chang, W. C. Cloning and sequencing of a carp beta S-crystallin cDNA. *Biochim. Biophys. Acta* **1987**, *910*, 89–92.
- (38) Quax-Jeuken, Y.; Driessen, H.; Leunissen, J.; Quax, W.; de Jong, W.; Bloemendal, H. Beta S-crystallin: structure and evolution of a distinct member of the  $\beta\gamma$ -superfamily. *Eur. Mol. Biol. Org. J.* **1985**, *4*, 2597–2602.
- (39) van Rens, G. L.; de Jong, W. W.; Bloemendal, H. One member of the  $\gamma$ -crystallin gene family,  $\gamma$ S, is expressed in birds. *Exp. Eye Res.* **1991**, *53*, 135–138.
- (40) van Rens, G. L.; Raats, J. M.; Driessen, H. P.; Oldenburg, M.; Wijnen, J. T.; Khan, P. M.; de Jong, W. W.; Bloemendal, H. Structure of the bovine eye lens  $\gamma$ S-crystallin gene (formerly  $\beta$ S). *Gene* **1989**, *78*, 225–233.
- (41) Altschul, S.; Madden, A.; Madden, T.; Schaffer, A.; Zhang, J.; Zhang, Z.; Miller, W.; Lipman, D. Gapped BLAST and PSI-Blast: a new generation of protein database search programs. *Nucleic Acids Res.* **1997**, *25*, 3389–3402.
- (42) Wistow, G.; Wyatt, K.; David, L.; Gao, C.; Bateman, O.; Bernstein, S.; Tomarev, S.; Segovia, L.; Slingsby, C.; Vihtelic, T.  $\gamma$ N-crystallin and the evolution of the  $\beta\gamma$ -crystallin superfamily in vertebrates. *Fed. Soc. Biochem. Mol. Biol.* **2005**, *272*, 2276–2291.
- (43) Howe, K.; et al. The zebrafish reference genome sequence and its relationship to the human genome. *Nature* **2013**, *496*, 498–503.
- (44) Chiou, S.-H.; Pan, F.-M.; Peng, H.-W.; Chao, Y.-K.; Chang, W.-C. Characterization of  $\gamma$ S-crystallin isoforms from a catfish: evolutionary comparison of various  $\gamma$ -,  $\gamma$ S-, and  $\beta$ -crystallins. *Biochem. Biophys. Res. Commun.* **1998**, *252*, 412–419.
- (45) Pan, F. M.; Chuang, M. H.; Chiou, S. H. Characterization of  $\gamma$ S-crystallin isoforms from lip shark (*Chiloscyllium colax*): evolutionary comparison between  $\gamma$ S and  $\beta/\gamma$  crystallins. *Biochem. Biophys. Res. Commun.* **1997**, *240*, 51–56.
- (46) Bowie, J. U.; Reidhaar-Olson, J. F.; Lim, W. A.; Sauer, R. T. Deciphering the message in protein sequences: tolerance to amino acid substitutions. *Science* **1990**, *247*, 1306–1310.
- (47) Hormoz, S. Amino acid composition of proteins reduces deleterious impact of mutations. *Sci. Rep.* **2013**, *3*, 2919.
- (48) Szilágyi, A.; Závodszy, P. Structural differences between mesophilic, moderately thermophilic, and extremely thermophilic protein subunits: results of a comprehensive survey. *Structure* **2000**, *8*, 493–503.
- (49) Budiman, C.; Koga, Y.; Takano, K.; Kanaya, S. FK506-binding protein 22 from a psychrophilic bacterium, a cold shock-inducible peptidyl prolyl isomerase with the ability to assist in protein folding. *Int. J. Mol. Sci.* **2011**, *12*, 5261–5284.
- (50) Kyte, J.; Doolittle, R. A simple method for displaying the hydropathic character of a protein. *J. Mol. Biol.* **1982**, *157*, 105–132.
- (51) Gasteiger, E.; Hoogland, C.; Gattiker, A.; Duvaud, S.; Wilkins, M. R.; Appel, R. D.; Bairoch, A. Protein Identification and Analysis Tools on the ExPASy Server. In *The Proteomics Protocols Handbook*; Walker, J. M., Ed.; Humana Press: Totowa, NJ, 2005; pp 571–607.
- (52) Ikai, A. Thermostability and aliphatic index of globular proteins. *J. Biochem.* **1980**, *88*, 1895–1898.
- (53) Zhou, X. X.; Wang, Y. B.; Pan, Y. J.; Li, W. F. Differences in amino acids composition and coupling patterns between mesophilic and thermophilic proteins. *Amino Acids* **2008**, *34*, 25–33.
- (54) Metpally, R. P. R.; Reddy, B. V. B. Comparative proteome analysis of psychrophilic versus mesophilic bacterial species: insights into the molecular basis of cold adaptation of proteins. *BMC Genomics* **2009**, *10*, DOI: 10.1186/1471-2164-10-11.
- (55) Chakravarty, S.; Varadarajan, R. Elucidation of determinants of protein stability through genome sequence analysis. *FEBS Lett.* **2000**, *470*, 65–69.
- (56) Jones, D. T. Protein secondary structure prediction based on position-specific scoring matrices. *J. Mol. Biol.* **1999**, *292*, 195–202.
- (57) Buchan, D. W. A.; Minnici, F.; Nugent, T. C. O.; Bryson, K.; Jones, D. T. Scalable web services for the PSIPRED protein analysis workbench. *Nucleic Acids Res.* **2013**, *41*, W340–W348.
- (58) Brubaker, W. D.; Freitas, J. A.; Golchert, K. J.; Shapiro, R. A.; Morikis, V.; Tobias, D. J.; Martin, R. W. Separating instability from aggregation propensity in  $\gamma$ S-crystallin variants. *Biophys. J.* **2011**, *100*, 498–506.
- (59) Chen, J.; Callis, P.; King, J. Mechanism of the very efficient quenching of tryptophan fluorescence in human  $\gamma$ D- and  $\gamma$ S-crystallins: The  $\gamma$ -crystallin fold may have evolved to protect tryptophan residues from ultraviolet photodamage. *Biochemistry* **2009**, *48*, 3708–3716.
- (60) Vajpai, N.; Nisius, L.; Wiktor, M.; Grzesiek, S. High-pressure NMR reveals close similarity between cold and alcohol protein denaturation in ubiquitin. *Proc. Natl. Acad. Sci. U.S.A.* **2013**, *110*, E368–E376.

- (61) Babu, C.; Hilser, V.; Wand, A. Direct access to the cooperative substructure of proteins and the protein ensemble via cold denaturation. *Nat. Struct. Mol. Biol.* **2004**, *11*, 352–357.
- (62) Jaremko, M.; Jaremko, Ł.; Kim, H.-Y.; Cho, M.-K.; Schwieters, C. D.; Giller, K.; Becker, S.; Zweckstetter, M. Cold denaturation of a protein dimer monitored at atomic resolution. *Nat. Chem. Biol.* **2013**, *9*, 264–270.
- (63) Annunziata, O.; Ogun, O.; Benedek, G. B. Observation of liquid-liquid phase separation for eye lens  $\gamma$ S-crystallin. *Proc. Natl. Acad. Sci. U.S.A.* **2003**, *100*, 970–974.
- (64) Liu, C.; Asherie, N.; Lomakin, A.; Pande, J.; Ogun, O.; Benedek, G. B. Phase separation in aqueous solutions of lens  $\gamma$ -crystallins: special role of  $\gamma$ S. *Proc. Natl. Acad. Sci. U.S.A.* **1996**, *93*, 377–382.
- (65) Posner, M.; Kiss, A. J.; Skiba, J.; Drossman, A.; Dolinska, M. B.; Hejtmancik, J. F.; Sergeev, Y. V. Functional validation of hydrophobic adaptation to physiological temperature in the small heat shock protein  $\alpha$ A-crystallin. *PLoS One* **2012**, *7*, e34438.
- (66) Bennion, B. J.; Daggett, V. The molecular basis for the chemical denaturation of proteins by urea. *Proc. Natl. Acad. Sci. U.S.A.* **2003**, *100*, 5142–5147.
- (67) Monera, O. D.; Kay, C. M.; Hodges, R. S. Protein denaturation with guanidine hydrochloride or urea provides a different estimate of stability depending on the contributions of electrostatic interactions. *Protein Sci.* **1994**, *3*, 1984–1991.
- (68) O'Brien, E. P.; Dima, R. I.; Brooks, B.; Thirumalai, D. Interactions between hydrophobic and ionic solutes in aqueous guanidinium chloride and urea solutions: lessons for protein denaturation mechanism. *J. Am. Chem. Soc.* **2007**, *129*, 7346–7353.
- (69) Koishi, T.; Yasuoka, K.; Willow, S. Y.; Fujikawa, S.; Zeng, X. C. Molecular insight into different denaturing efficiency of urea, guanidinium, and methanol: a comparative simulation study. *J. Chem. Theory Comput.* **2013**, *9*, 2540–2551.
- (70) Hédoux, A.; Krenzlin, S.; Paccou, L.; Guinet, Y.; Flamentad, M.-P.; Siepmann, J. Influence of urea and guanidine hydrochloride on lysozyme stability and thermal denaturation; a correlation between activity, protein dynamics and conformational changes. *Phys. Chem. Chem. Phys.* **2010**, *12*, 13189–13196.